

# EVOLUTION OF GLAZE POROSITY IN FIRING. SINTERING MECHANISM AND KINETICS.

(\*) Amorós, J.L.; Orts, M.J.; Gozalbo, A.; Belda, A.;  
(\*\*) Sanmiguel, F.; Rodrigo, J.L.; Fernando, V.

(\*) Instituto de Tecnología Cerámica (ITC).  
Asociación de Investigación de las Industrias Cerámicas (AICE)  
Universidad Jaume I. Castellón. Spain.  
(\*\*) TORRECID, S.A.

## ABSTRACT

A study was undertaken on the mechanism and kinetics of the process by which porosity is reduced in a glaze particle packing (sintering), in an intent to maximise porosity reduction in the resulting fired glaze coating. The study was carried out by using a frit particle distribution of an entirely glassy nature, obtained from a standard glass, and three particle-size distributions taken from a single glaze, prepared with a zirconium frit and kaolin. These materials underwent isothermal treatments and constant-rate heating. A semi-empirical equation was derived, which suitably describes glaze particle sintering kinetics. Moreover, scanning electron microscopy and mercury porosizing allowed determining the mechanism that gives rise to sealed pore formation in a glaze, and establishing how unfired glaze particle-size distribution impacts final glaze porosity.

## 1 INTRODUCTION

During the firing of ceramic glazes, frit particle viscosity progressively drops as temperature rises. These frit particles agglomerate or coalesce as a result of the capillary pressure that arises at their contact points, which leads to increased shrinkage of the material, and a change in the original porous texture (decreased pore volume and changes in pore size and shape). In advanced process states, porosity still remains basically apparent, while in the final states, at low porosity values, porosity is mainly sealed, with pores containing occluded gas. In this process state, the material layer reaches minimum porosity, under given firing conditions, when the pressure of the trapped gases in the pores equals capillary pressure (process-driving force).

It follows therefore, that part of the porosity of a fired glaze coating is quite likely to stem from some of the pores that were already present in the newly applied glaze layer. It was thus decided to try and obtain more data than currently available, on the mechanism and kinetics involved in reducing porosity of a glaze particle packing in firing, in an intent to reduce final glaze porosity. This research was consequently designed and carried out with the following specific aims:

- i) Determination of the sintering mechanism and kinetics of a frit particle packing of an exclusively glassy nature. This was done by conducting a set of isothermal and nonisothermal experiments (at constant-rate heating), using test specimens formed from standard glass particles, whose viscosity in the melt had been accurately determined.
- ii) Determination of the sintering mechanism and kinetics of a zirconium glaze, assessing the influence of its particle-size distribution on the process rate and upon final glaze porosity.

**1.1 SINTERING OF GLAZE PARTICLE PACKINGS. PROPOSED KINETIC EQUATION.**

Although numerous theoretical models have been put forward for studying glass particle sintering, they are based on so many microstructural simplifications (constant-sized, sphered particles, regular particle packings, etc.), that they are only partially applicable to very simple systems (1-8). Therefore, in order to describe the sintering process of packings of irregularly shaped frit particles with a wide range of size distributions, empirical or semi-empirical equations are used (10)(9)(4). Thus, in view of the data reported by various workers, and the shape of the curves obtained on plotting material porosity against kiln dwell time in isothermal experiments, it was considered that the sintering rate (dX/dt) might be described by a semi-empirical equation of the type:

$$\frac{dX}{dt} = K(1 - X) \tag{1}$$

where:

X = the degree of sintering advance or degree of sintering, defined as:

$$X = \frac{\rho_c - \rho_0}{\rho_{max} - \rho_0} \tag{2}$$

where:

- $\rho_c$  = bulk density of the partially densified material.
- $\rho_0$  = unfired bulk density.
- $\rho_{max}$  = peak density.

The degree of sintering advance is represented by the ratio: already suppressed porosity/peak suppressible porosity. It has been defined in this fashion, because a material's final porosity is never cancelled out when peak densification is achieved.

Parameter K is the process rate constant. According to the theoretical kinetic models of viscous flow sintering, K must be proportional to glass surface tension ( $\sigma$ ), and inversely proportional to its viscosity ( $\eta$ ) and its particle radius (r).

$$K \propto \frac{\sigma}{\eta r} \tag{3}$$

Integrating Equation [1] within the limits for t=0, X=0 and for t=t, X=X, gives:

$$\ln\left(\frac{I}{I-X}\right) = Kt \quad [4]$$

Thus, if the results obtained in an isothermal experiment are plotted in the form  $\ln[1/(1-X)]$  vs.  $t$ , a straight should be found, which must pass through the origin, if the proposed kinetic equation is appropriate.

On attempting to establish a relationship between  $K$  and temperature, it may be assumed that variations in temperature will affect liquid-phase viscosity ( $\eta$ ) more than its surface tension ( $\sigma$ ). Bearing in mind that the variation of  $\eta$  with temperature may be described approximately for narrow temperature intervals by an exponential relation of the type:

$$\eta = A \cdot \exp\left(\frac{Q}{RT}\right) \quad [5]$$

and taking into account Equation [3], the relation between  $K$  and  $T$  is given by:

$$K = K_0 \cdot \exp\left(-\frac{Q}{RT}\right) \quad [6]$$

If the experiments are carried out at a constant rate of heating ( $a$ ), the following holds:

$$\frac{dt}{dT} = \frac{1}{a} \quad [7]$$

Thus, multiplying both members of Equation [1] by the reciprocal of the heating rate, yields the equation:

$$\frac{dX}{dT} = \frac{K}{a} (I-X) \quad [8]$$

Substituting Equation [6] into Equation [8] gives:

$$\frac{dX}{dT} = \frac{K_0}{a} \exp\left(-\frac{Q}{RT}\right) (I-X) \quad [9]$$

Making the assumption that the apparent activation energy of the process ( $Q$ ) and parameter  $K_0$  remain constant during the experiment, since they do not depend on temperature, Equation [9] can be integrated, thus yielding:

$$\ln\frac{I}{(I-X)} = \frac{K_0}{a} \frac{RT^2}{Q} \exp\left(-\frac{Q}{RT}\right) \quad [10]$$

Moving  $T^2$  to the first term of Equation [10] and taking logarithms, gives:

$$\ln\left[\frac{I}{T^2} \ln\left(\frac{I}{I-X}\right)\right] = \ln\frac{K_0}{a} \frac{R}{Q} - \frac{Q}{RT} \quad [11]$$

Therefore, if the proposed model is correct, plotting the values of the first member of Equation [11] versus  $1/T$  should yield a straight line, from whose slope  $(-Q/R)$  and ordinate at the intercept  $[\ln(K_0/a)(R/Q)]$ , the apparent activation energy of the sintering process ( $Q$ ) and the frequency factor ( $K_0$ ) can be calculated.

## 2 MATERIALS USED AND EXPERIMENTAL TECHNIQUE

### 2.1 MATERIALS USED

A NIST SRM-717 standard glass and three particle-size distributions of a single glaze were used. The glaze involved was prepared from an industrial zirconium frit to which 8% kaolin had been added.

*Table I. Test specimen particle mean diameter (D).*

Material	D( $\mu\text{m}$ )
Standard glass	13,5
Glaze. Fraction G	27,9
Glaze. Fraction M	18,3
Glaze. Fraction F	6,3

### 2.2 EXPERIMENTAL TECHNIQUE

#### 2.2.1 Sintering of standard glass test specimens under isothermal conditions

The standard glass was wet ground in a fast laboratory mill. The suspension obtained was dried and the resulting powder was pressed, forming 3 mm high cylindrical test specimens with a diameter of 25 mm. These test specimens were dried and isothermally fired at temperatures of: 625, 650 and 670 °C, with varying residence times ranging from 10-840 min.

The degree of sintering was determined by measuring the unfired bulk density of the specimens, which were subsequently fired at different temperatures and differing dwell times.

#### 2.2.2 Sintering at constant-rate heating

Sintering at constant-rate heating was done in a hot-stage microscope. The variation of the degree of sintering of the test specimen was determined by continuously monitoring the evolution of its geometry (by image analysis). Initially, the cylindrical test specimen had a 3 mm diameter and was 3 mm thick. The heating rates used were 2, 5 and 10°C/min.

### 3 RESULTS AND DISCUSSION

#### 3.1 SINTERING OF TEST SPECIMENS FORMED FROM STANDARD GLASS PARTICLES

##### 3.1.1 Isothermal experiments

##### 3.1.1.1 Process kinetics

Fig. 1 shows a plot of the degree of sintering ( $X$ ) which the standard glass specimens reached against kiln dwell time for the three isothermal heat treatments run. The values of  $X$  were calculated from the test specimen unfired bulk density values, which were practically constant ( $\rho_0 = 1,198\text{g/cc}$ ), from the fired bulk density of each test specimen ( $\rho_c$ ), and from the bulk density of the most compact test specimen ( $\rho_{\text{max.}} = 2,205\text{g/cc}$ ). The most sintered specimen was obtained on heating the sample at  $670^\circ\text{C}$  for 210 min. Its sealed porosity was determined from the density values of the glass, and bulk density of the test specimen was 2%.

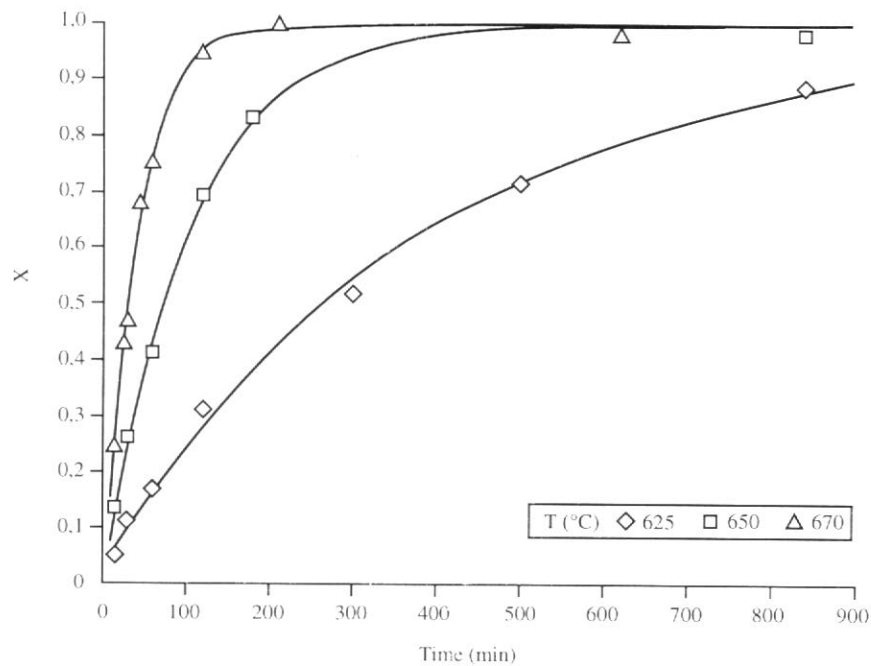


**Figure 1.** Variation of the test specimen degree of sintering with temperature and kiln dwell time. Standard glass.

Fig. 2 depicts a plot of the values  $\ln(1/(1-X))$  corresponding to each test specimen, versus kiln dwell time, for three temperatures. It can be observed that except for the values corresponding to the two test specimens that were fired at  $650^\circ\text{C}$  and  $670^\circ\text{C}$  for long periods of time, in which the gases occluded in the pores expanded, the results fit three straight lines quite satisfactorily, one for each tested temperature. The slope of these straight lines is positive and increases with temperature, in accordance with the proposed kinetic equation.

On plotting the values obtained for  $\ln K$ , versus those of the inverse of absolute temperature ( $1/T$ ) and those of the inverse of viscosity ( $1/\eta$ ) versus this same variable, two practically parallel straight lines were obtained (Fig. 3). These results confirm, on the one hand, that the effect of temperature on the sintering rate constant and on viscosity can be described by an Arrhenius-type equation (Equations [5] and [6]). On the other hand, they

show that the sintering process rate constant is inversely proportional to glass viscosity, just as predicted by the models for particle sintering by viscous flow. A plot is shown in Fig. 1, by means of solid lines, of how the degree of sintering of the test specimens evolves with kiln dwell time for the three tested temperatures, calculated from the proposed kinetic equation. It can be observed, that the experimental data and the computed values match well.

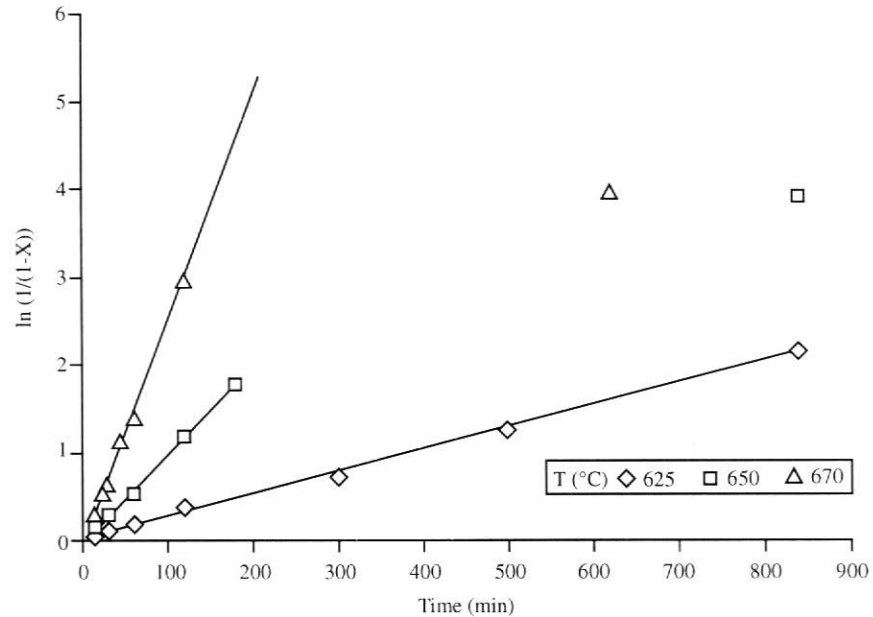


Figure 2. Fit of the data to proposed kinetic Equation [4]. Standard glass.

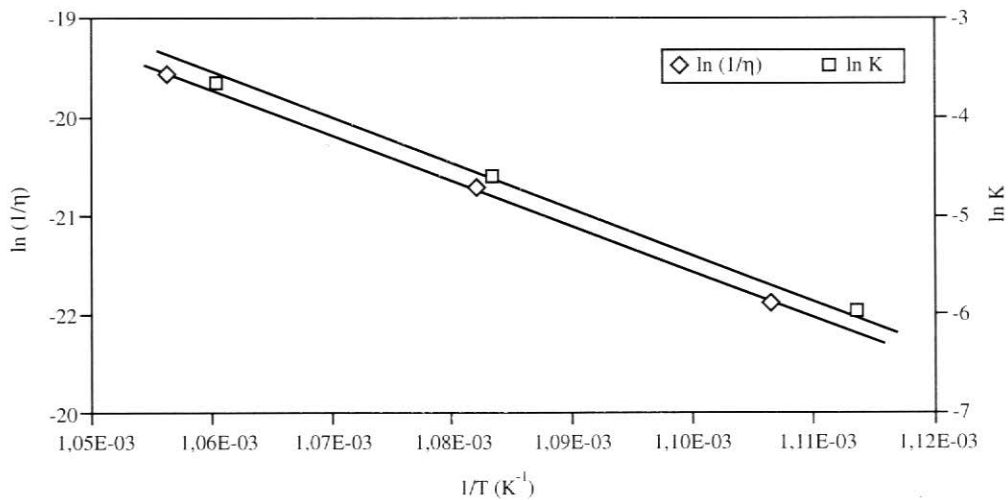
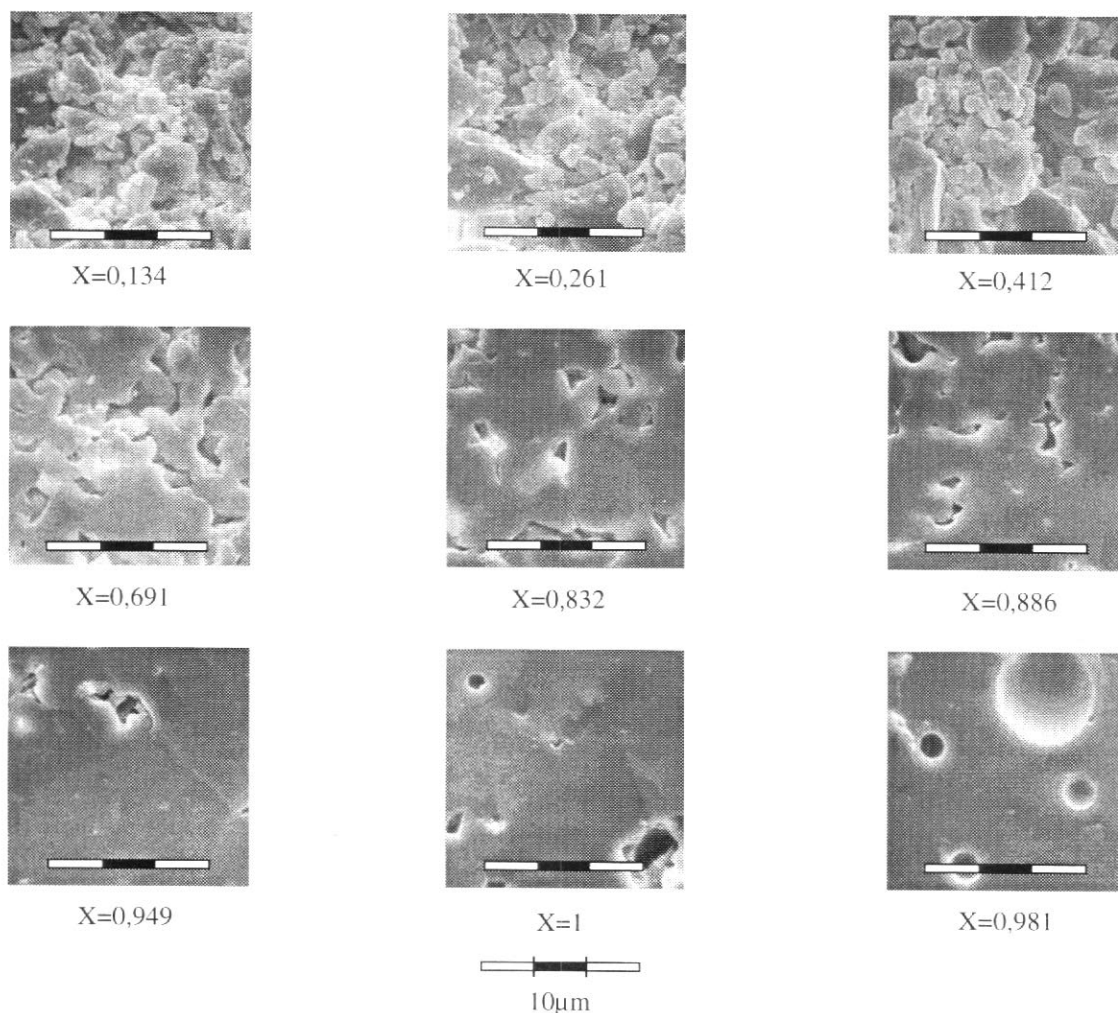


Figure 3. Influence of temperature on rate constant (K) and on the inverse of viscosity (1/η). Standard glass.

### 3.1.1.2 Evolution of the microstructure of the test specimen with the degree of sintering advance

Fig. 4 depicts the microphotographs corresponding to test specimens with different degrees of sintering (X), obtained at various temperatures and kiln dwell times.



**Figure 4.** Microphotographs corresponding to test specimens with a different degree of sintering ( $X$ ), obtained from standard glass particles.

On examining the test specimens obtained using different heat treatments by scanning electron microscopy (SEM), it was observed that the relation between the microstructure of the test pieces and the degree of sintering advance ( $X$ ), which is shown in Fig. 4, is independent of the heat-treatment cycle employed. An analogous conclusion may be drawn from Fig. 5, in which the variation of the apparent pore mean diameter ( $D_p$ ) and the ratio: apparent porosity/sealed porosity of the test specimens versus the degree of sintering advance ( $X$ ) have been plotted. On plotting the values of  $D_p$  of the test specimens, fired at different temperatures and kiln dwell times, versus the corresponding values of ( $X$ ), a single curve is found. The same occurs with the ratio apparent porosity/sealed porosity.

For values of  $X < 0,5$ , in Fig. 4, it can be observed that as sintering advances,  $X$  increases, glass particle mean size grows, mainly owing to the progressive disappearance of the smallest particles. In fact, at the contact points between the small particles, and between the small particles and the largest ones, higher capillary pressures arise than in the others, which leads to agglomerates with small particles densifying faster than the rest. Moreover, it can be observed that as the process advances, the glass particle edges become more rounded, since the system's surface energy is also lowered in this manner. In this initial sintering stage, porosity is apparent and mean pore size grows as the process advances (Fig. 5). Actually, the smallest pores (voids between small particles) are progressively suppressed while the volume of the medium-sized pores rises (Fig. 6). This rise in mean

and most common pore size occurs because the decrease in the smallest pores produces differential shrinkage in particle packings with a wide size distribution (12).

In more advanced process states (Fig. 4), for values of  $X > 0,6$ , glass particles lose their identity and the material can be considered as a set of differently shaped and sized pores. The figure shows that the pores which initially form an interconnected capillary network, progressively close and sphere, until they become sealed and sphered in the final process states. It can also be observed that as the degree of sintering of the test specimen increases ( $X$ ), mean pore size and pore number progressively decrease until reaching minimum values at test specimen peak densification. However, at any sintering state, large pores can always be observed, since the rate at which these pores shrink is very low or even zero, because the capillary pressure that is produced inside them is also very small. If heat treatment is continued beyond an optimum value, mean pore size grows as a result of the expansion of the gases trapped within the pore ( $X=0,981$  in Fig. 4).

On comparing these results with the ones found by mercury porosizing (Fig. 5), for high degrees of sintering ( $X > 0,6$ ), the mercury porosizing technique is shown to produce important errors in determining pore sizes, since the capillaries do not have a circular cross section, nor is their radius constant. Furthermore, this technique does not allow detecting large-sized pores linked to smaller ones, because the volume of mercury that penetrates into these large pores is indirectly assigned to the pores with a smaller cross section to which they are linked (intrusion radii). It may thus be inferred that the mean pore diameter values obtained by mercury porosizing are lower than they really are, especially at high degrees of sintering. With regard to the variation of the ratio: apparent porosity/true porosity with the degree of sintering, the data are consistent with the SEM outcomes.

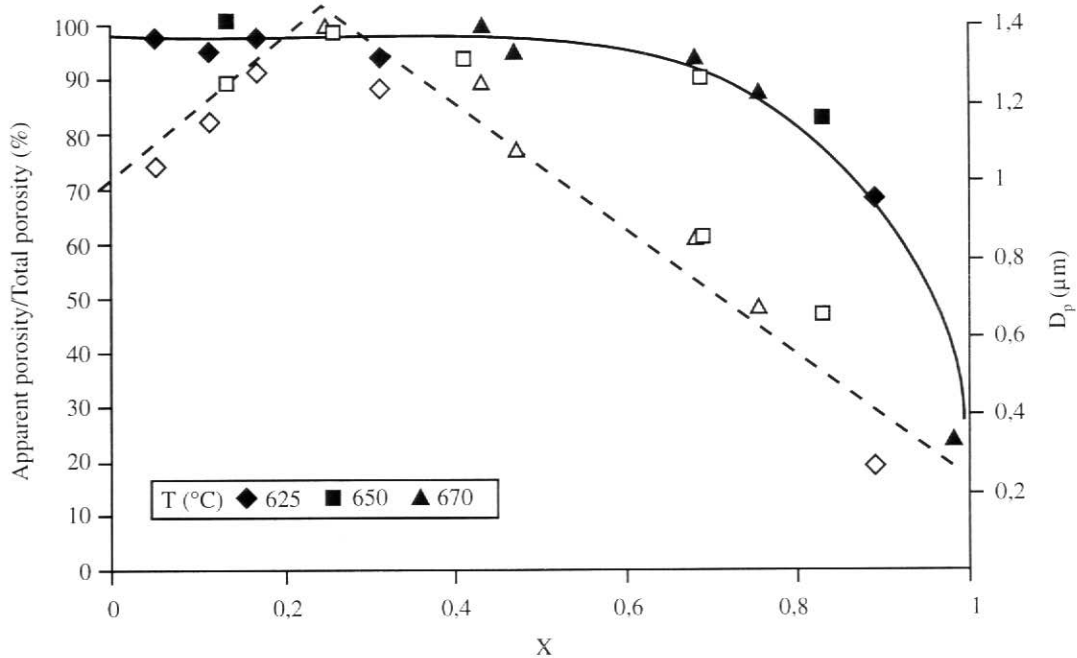


Figure 5. Variation of the ratio apparent porosity/true porosity (-) and apparent pore mean size (- -) with the degree of sintering advance. Standard glass.

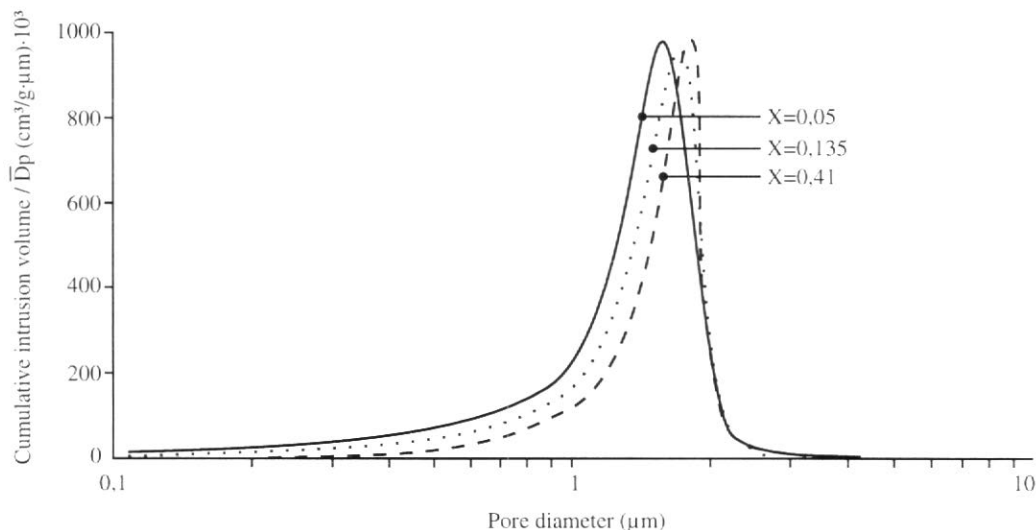
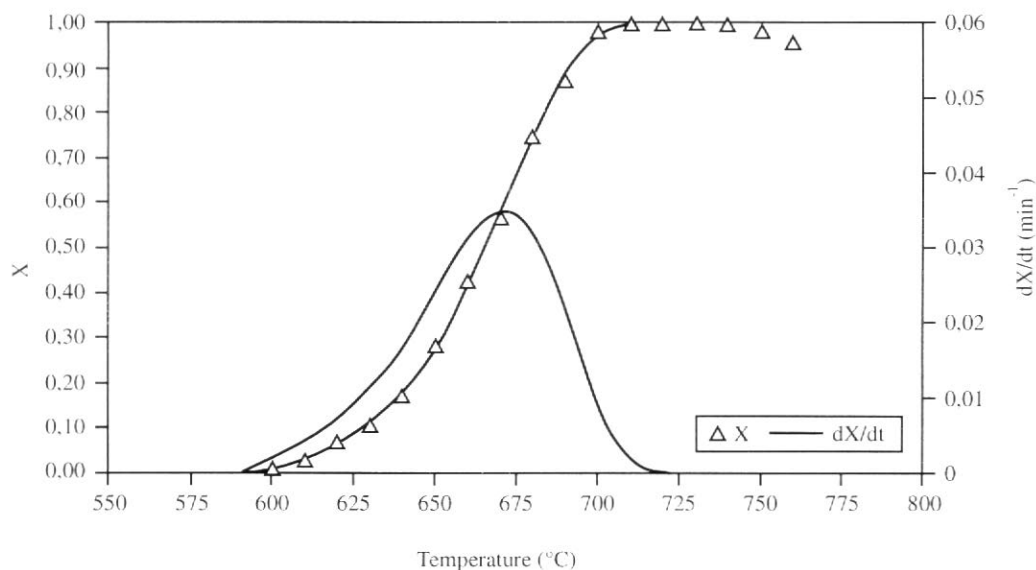


Figure 6. Evolution of apparent pore-size distribution with the degree of sintering advance. Standard glass.

### 3.1.2 Constant-rate heating experiments.

The results have been plotted in Fig. 7, which were obtained on heating a standard glass test specimen in the hot-stage microscope at a rate of 2°C/min, in the form, degree of sintering (X) versus temperature. The resulting curve has the typical sinusoidal shape of the proposed kinetic equation, up to peak densification, at a given temperature. If test specimen heating is continued, porosity rises (X decreases), owing to expansion of the occluded gases within the pores. The pairs of values, degree of test specimen sintering (X)-temperature (T), fit Equation [1] very well, which is the kinetic equation representing sintering at constant-rate heating (a). On fitting these values by linear regression to this equation, the apparent activation energy values of the process ( $Q=340\text{kJ/mol}$ ) and frequency factor ( $K_0=3,8 \cdot 10^{17} \text{min}^{-1}$ ) were obtained. With the fitted values of  $K_0$  and  $Q$ , the curves of the variation of the degree of conversion (X) with temperature, and the sintering rate ( $dX/dt$ ), versus this same variable were calculated. Fig. 7 shows that the match between the calculated values and the experimental data is excellent.



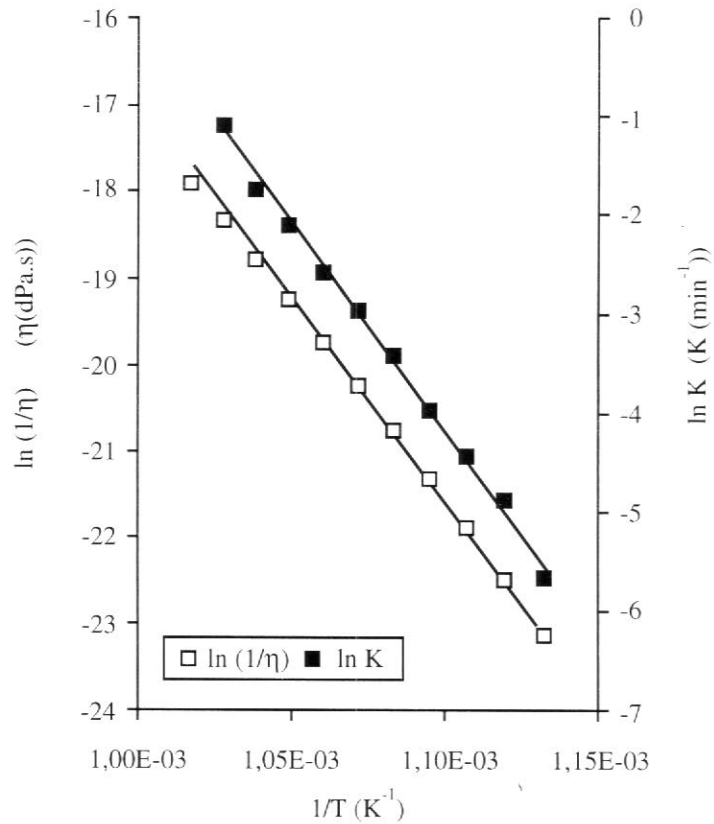
**Figure 7.** Evolution of the degree of sintering and sintering rate with temperature. Experiment at heating rate " $\alpha$ " = 2 °C/min. Standard glass.

Fig. 8 shows a plot of the experimentally obtained log. values of the rate constant (K), and those of the log. of the inverse of viscosity ( $1/\eta$ ), determined for this glass, versus the inverse of absolute temperature ( $1/T$ ). As was to be expected, two practically parallel straight lines were obtained. This once again substantiates that the marked effect of temperature on the glass particle sintering rate, described by the Arrhenius equation, occurs exclusively because glass viscosity decreases with temperature, exactly following the same trend.

On the other hand, these data show the suitability of the experimental technique employed for the study of the sintering of glass particle packings, since a heat treatment based on constant-rate heating of the test specimen is more like the heat treatment used industrially for firing glazes than an isothermal treatment. Furthermore, in order to determine the influence of temperature on the process rate by isothermal methods, at least three experiments are required, whereas this information can be obtained from a single experiment conducted at a constant rate of heating.

In this section, a low rate of heating was chosen (2 °C/min), so as to reduce temperature gradients within the test specimen as far as possible, and bring the specimen's temperature as close as possible to that registered by the kiln thermocouple of the hot-stage microscope. These conditions were suitable for attempting to verify the proposed kinetic equation and confirm whether the influence of temperature on the velocity constant was exclusively due to the dependence of glass viscosity on this variable.

Having satisfied these objectives, experiments were conducted at higher heating rates, although we were aware that on not obeying the foregoing requirements, the results might be partially distorted.



**Figure 8.** Influence of temperature on rate constant (K) and on the inverse of viscosity (1/η). Experiment at a constant rate of heating  $\alpha=2^\circ\text{C/min}$ . Standard glass.

The results obtained on using different heating rates have been plotted in Fig. 9. The curves are alike but have progressively shifted towards higher temperatures, as the heating rate rose. The data also fit the proposed kinetic equation (Equation 11). However, the activation energy values obtained on using heating rates of 5 and 10°C/min, are slightly higher than the corresponding value in the experiment with 2°C/min. This is probably because the difference between test specimen temperature and that recorded by the thermocouple rises as the heating rate increases.

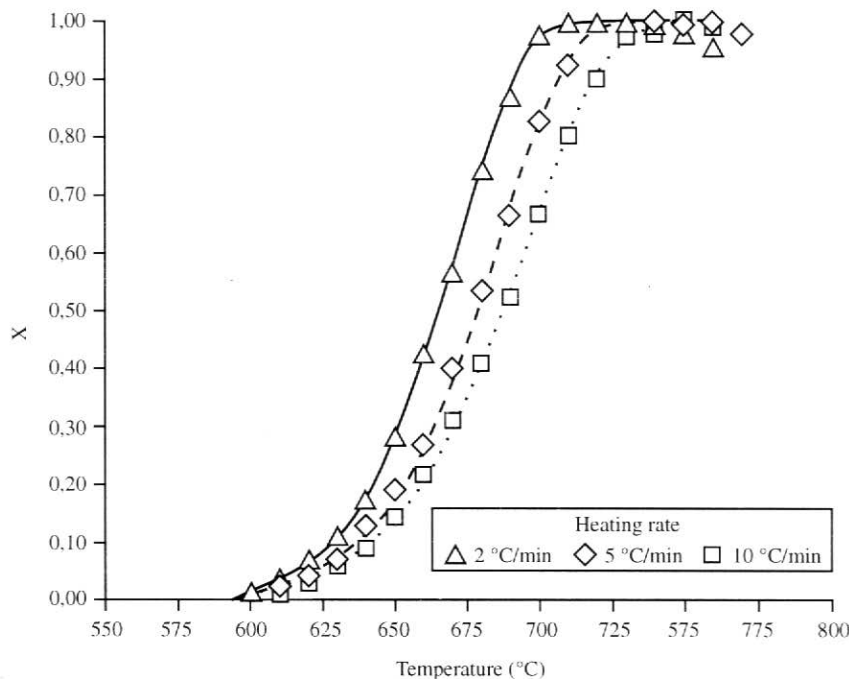
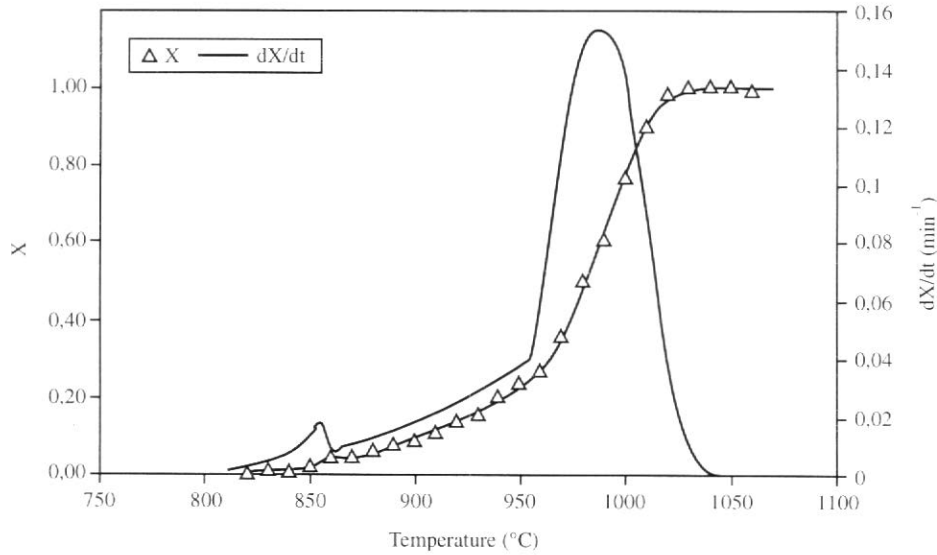


Figure 9. Influence of the heating rate on the degree of sintering. Standard glass.

### 3.2 SINTERING AT CONSTANT-RATE HEATING OF TEST SPECIMENS FORMED FROM A ZIRCONIUM GLAZE

#### 3.2.1 Experiments with a monosize particle distribution (Particle-size distribution M)

Fig. 10 shows a plot of the resulting data in the form: degree of sintering (X) versus temperature (T). Although the curve looks like the one obtained with the standard glass, there are some differences. This curve exhibits three stretches in which the variation of X with T does not follow the same trend. This becomes even clearer on plotting the first member of Equation [11] against the inverse of temperature (Fig. 11). This plot is not a straight line, unlike what happened with the corresponding glass plot. This shows that the kinetic equation that was valid for glasses is not directly applicable to this frit for the whole sintering process. However, three straight segments can be clearly identified in the plot, which indicates that for each temperature interval, the results fit the proposed kinetic equation well, although with different values for the activation energy (Q) and frequency factor ( $K_0$ ), since the slopes of these stretches also differ.



**Figure 10.** Evolution of the degree of sintering and sintering rate with temperature. Experiment at heating rate "a"=10°C/min. Glaze.

Linear fitting was used to determine the values of  $K_0$  and  $Q$  corresponding to each of these temperature intervals. With these values and Equation [11], the evolution was calculated of the sintering rate with temperature (Fig. 10).

In Fig. 11, it can also be observed that at the temperature interval between 850 and 950°C, the influence that temperature has on the rate constant (slope of the second stretch), and therefore on glaze effective viscosity, is much less that for the remaining temperatures (slope of the first and third stretches). This suggests that in the temperature range 850-950°C, extensive crystalline-phase devitrification must arise. In fact, crystal precipitation at the surface or inside the glass particles partially counteracts the decrease in viscosity in the glassy phase with the rise in temperature (13).

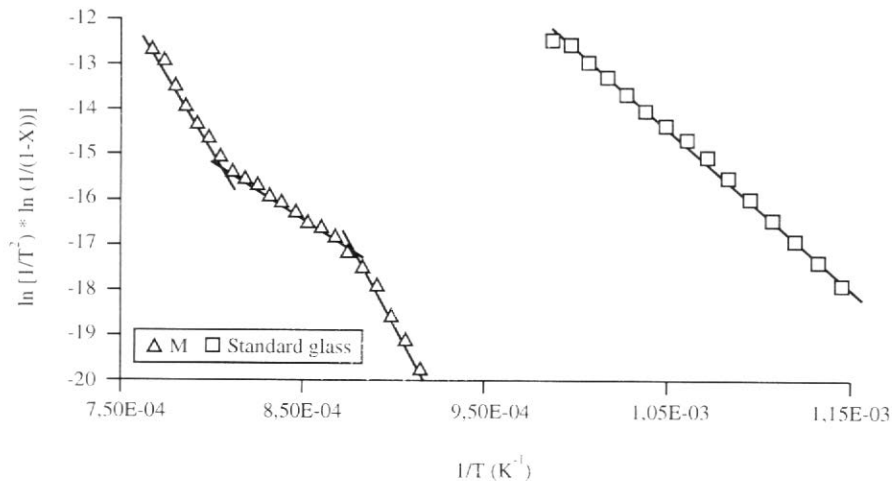


**Figure 11.** Fit of the experimental data to Equation [11]. Heating rate "a"=10°C/min. Particle-size distribution M.

To verify this assumption, a differential thermal analysis test was run on the glaze particles, at the same heating rate that was used in the sintering experiment (Fig. 12). A wide band can be observed in this thermogram, typical of surface crystallization, which commences at round 850°C and extends up to about 1000°C. It was shown by X-ray

diffraction that the crystallizing phases were a double silicate of calcium and magnesium, a double silicate of calcium and zinc, and zirconium silicate.

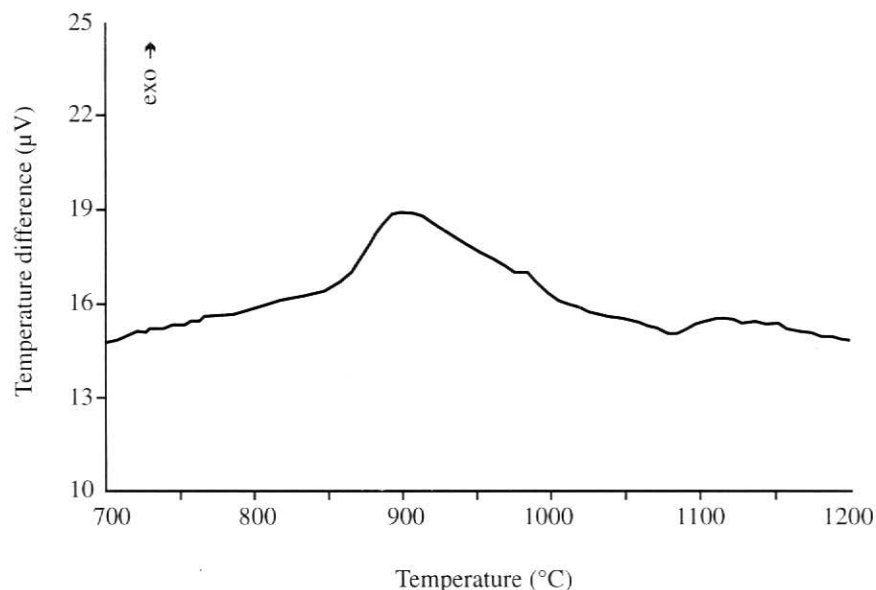


**Figure 12.** Thermogram corresponding to the zirconium glaze. Heating rate "a" = 10 °C/min. Particle-size distribution M.

These findings allowed concluding that this glaze sintered according to the mechanism set out below.

At temperatures below the start of frit devitrification (850 °C), the frit particles have an exclusively glassy nature, which is why their viscosity drops as temperature rises, entailing an increase in the densification rate of the test specimen (Fig. 10). Above 850 °C, crystalline phases start devitrifying, probably from the particle surfaces (13), at a rate that climbs with temperature until peaking at round 900 °C (crystallization peak in the thermogram). While crystallization continues at a considerable rate (between 850 and 950 °C), although the viscosity of the glassy phase keeps dropping with rising temperature, progressive crystal growth in the particles tends to raise effective viscosity (lowering deformability). The outcome of these opposite effects makes the system's effective viscosity decrease relatively little with rising temperature. A hike in temperature therefore gives rise to a slight increase in the sintering rate constant (Fig. 11) and the rate of this process (Fig. 10).

At higher temperatures (above 950 °C), the crystallization rate is already very low, so that the slight increase in the crystal proportion that arises hardly affects the marked drop in viscosity of the residual glassy phase with increased temperature. Consequently, the sintering rate constant rises considerably with temperature until the test specimen reaches peak densification (final stretch of Fig. 11). The sintering rate follows this trend up to values for the degree of sintering (X) approaching 0,7 (Fig. 10). If temperature keeps on rising, the densification rate progressively falls until it cancels out, just as occurred in the case where sintering was involved of particles of an exclusively glassy nature, discussed in the foregoing section.

The evolution that the porous texture of the test specimen undergoes as sintering advances is quite like that observed in the case of the glass particles (Section 3.1.1.2). Fig. 13 shows some selected microphotographs of this glaze.

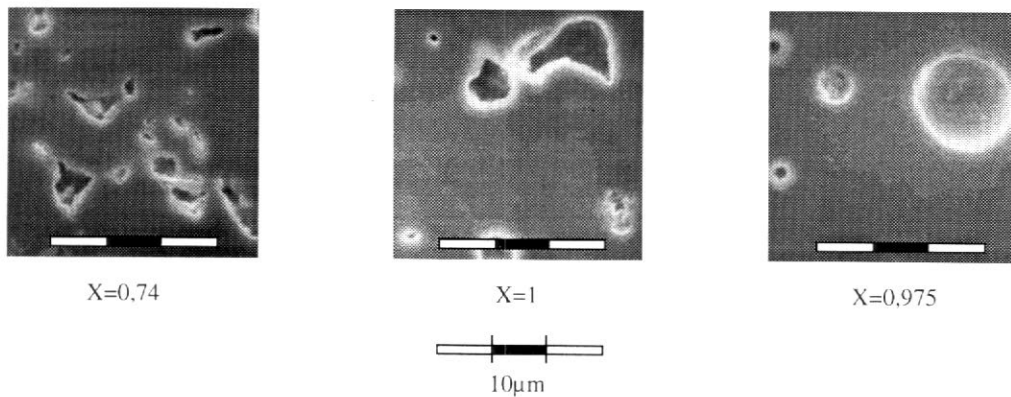


Figure 13. Microphotographs corresponding to test specimens with different degrees of sintering ( $X$ ), obtained from the zirconium frit. Particle-size distribution M.

### 3.2.2 Experiments with different particle-size distributions

On modifying the particle-size distribution of a glaze, porosity and pore-size distribution in the resulting particle packing are also altered. As may be observed in Fig. 14, that as mean size is reduced and the width of the particle-size distribution increases, pore volume rises in the unfired test specimen. However, the width of the test specimen's pore-size distribution and its mean pore diameter are reduced, as the size and volume of the coarsest pores are decreased. Thus, the resulting particle packing with the finest particle-size distribution (F) exhibits the highest porosity, and is at the same time the most uniform, since maximum pore size (intrusion diameter) lies below  $1\mu\text{m}$ .

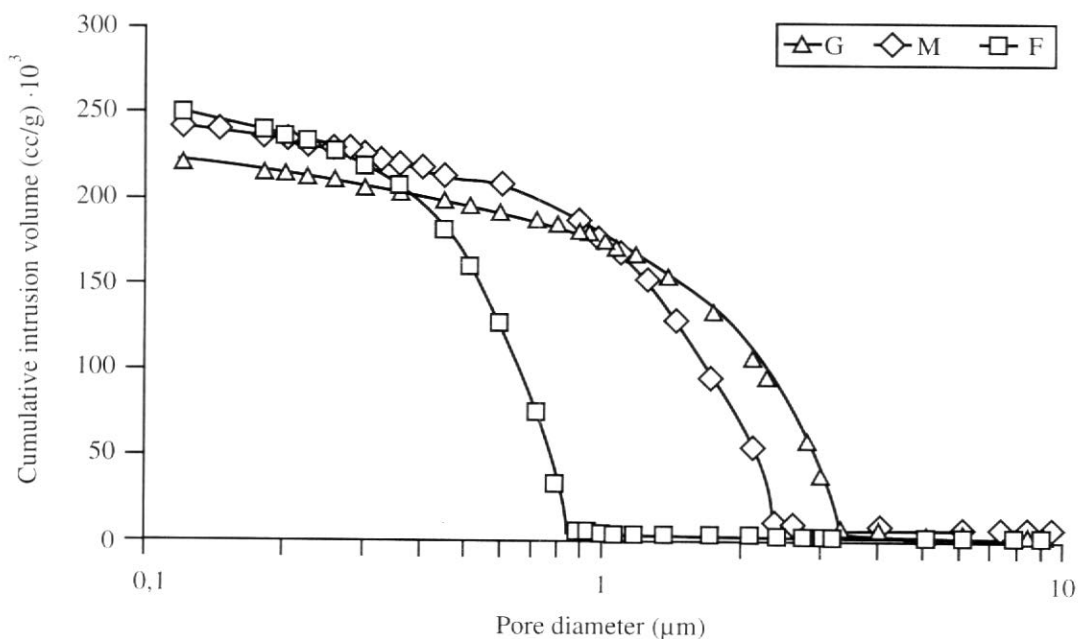


Figure 14. Pore-size distribution of the unfired test specimens corresponding to particle-size distributions G, M, and F.

Alterations in mean particle and pore sizes in an unfired packing and its microstructural uniformity, obtained by modifying glaze particle-size distribution may therefore be expected to considerably affect not just the rate at which the material densifies, but also its porous structure in the different process states.

The plot has been depicted in Fig. 15 of the curves of the degree of sintering (X)-temperature (T), corresponding to the test specimens formed from glaze particle-size distributions G, M and F. The curves are similar, but have shifted towards higher temperatures as mean particle size (D) of the particle-size distribution increased. Just as in the previous section, for particle-size distribution M, it has been attempted to fit the pairs of values degree of sintering (X)-temperature (T) corresponding to glaze particle-size distributions G and F to Equation [11]. Two broken straight lines were obtained, one for each particle-size distribution, each having three straight stretches, analogous to the plot shown in Fig. 12.

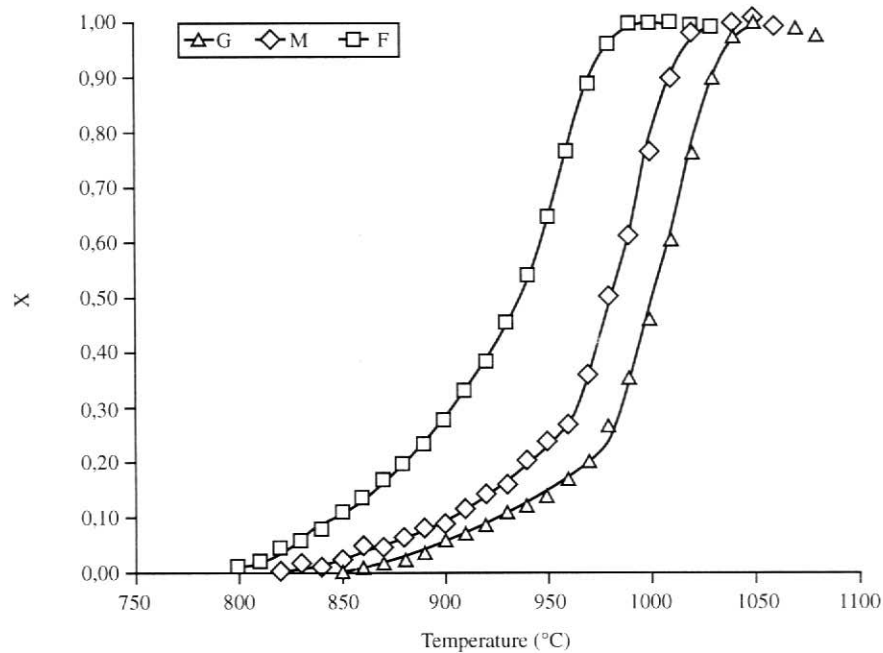


Figure 15. Influence of glaze particle-size distribution on the degree of sintering.

Table II details the values of the temperature intervals, energy activation (Q) and frequency factor (K<sub>0</sub>) for particle-size distributions G, M, and F, for each curve stretch.

Table II. Kinetic parameters corresponding to the three glaze particle-size distributions.

Stretch	Particle-size distribution	Temperature interval (°C)	K <sub>0</sub> (min <sup>-1</sup> )	Q (kJ/mol)
I	F	800-840	6,5.10 <sup>25</sup>	575
	M	820-860	6,9.10 <sup>24</sup>	574
	G	850-890	1,5.10 <sup>24</sup>	575
II	F	840-940	3,2.10 <sup>8</sup>	218
	M	860-960	7,5.10 <sup>7</sup>	216
	G	900-980	3,1.10 <sup>7</sup>	215
III	F	940-990	2,0.10 <sup>22</sup>	531
	M	960-1040	4,8.10 <sup>21</sup>	533
	G	980-1060	3,1.10 <sup>21</sup>	535

An analysis of these data (Fig. 15 and Table II) shows that as mean size and width of the particle-size distribution decrease, the sintering rate of the particles rises considerably, which means in constant-rate-of-heating experiments, that the temperature at which the

test specimen reaches a given degree of densification drops considerably. Thus, particle-size distribution F attains minimum porosity round 990°C, at a temperature that is 50°C lower than the one corresponding to distribution M, which has a particle-size distribution similar to the one used industrially (Fig. 15). However, the coarsest one reaches minimum porosity at round 1060°C. The influence of the glaze particle-size distribution on the sintering rate at any process state can be better quantified by means of the value of  $K_0$  (Table II). It can be observed that the values of the frequency factor ( $K_0$ ), and therefore process rate increase as mean particle size and the width of particle-size distribution are decreased.

The marked effect that glaze particle-size distribution has upon the process rate stems from the fact that the capillary pressure (sintering-driving force), which arises within the pores and at the interparticle contact points, becomes greater as particle and pore sizes decrease.

It can furthermore be observed that glaze particle-size distribution does not alter the effect that temperature has on the process rate. Thus, for each of the three stretches, the value of the apparent activation energy remains virtually constant. This underscores once again the fact that the effect of temperature on the sintering rate is exclusively due to the influence of this variable on molten glaze viscosity, since this property must, in principle, depend very little on starting glaze particle size.

Fig. 16 shows a plot, for each glaze particle-size distribution of the variation that apparent pore mean size undergoes ( $D_p$ ) with the degree of glaze sintering advance. In the initial material densification stages, porosity is practically apparent, so that the results obtained by mercury porosizing are not unduly biased and may be used to compare the behaviour of the three particle-size distributions.

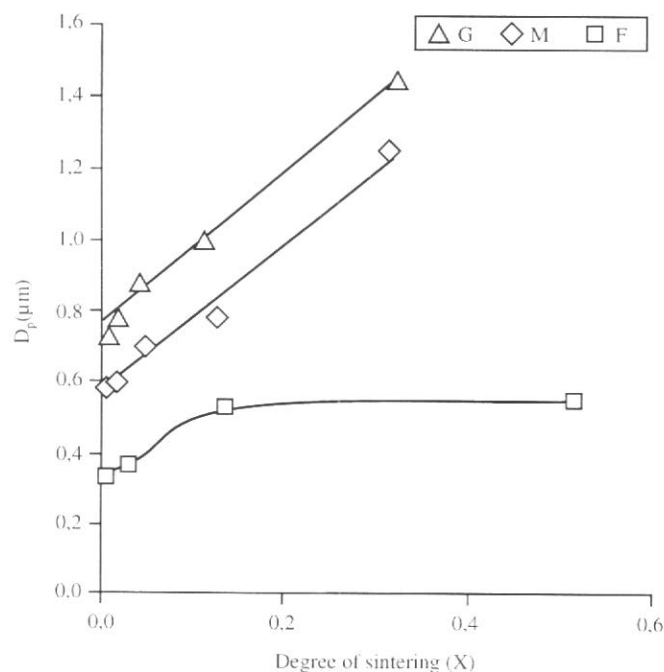


**Figure 16.** Variation of apparent pore mean size ( $D_p$ ) with the degree of sintering advance for each studied particle-size distribution.

It can be observed that the increase of mean pore size, which occurs while the glaze sinters, becomes greater with increased nonuniformity of the microstructure of the unfired

test specimen, in accordance with what has been set out in Section (3.2.2). The growth of mean pore size ( $D_p$ ) corresponding to the test specimen formed with distribution F, which is the most uniform, is very small. The opposite occurred with distributions M and G.

The greater or lesser uniformity of the microstructure of the unfired particle packing, caused by using more or less wide particle-size distributions, has an even greater impact on the porous structure of the glaze layer in the final firing stage, as shown in Table III. The table summarizes the values of sealed porosity, and other parameters that characterize the porous structure, corresponding to the glaze test specimens that were fired to peak densification (minimum porosity), for the three tested particle-size distributions.

*Table III. Porosity of the test specimens formed from distributions F, M and G and fired to peak density.*

<b>Particle-size distribution</b>	<b>Firing temperature (°C)</b>	<b>Porosity (%)</b>	<b>Pore mean diameter (µm)</b>	<b>Pore volume of <math>D_v &gt; 20\mu\text{m}</math> /solid volume (%)</b>
<b>F</b>	990	0,7	7,6	0,05
<b>M</b>	1040	2,1	8,8	0,16
<b>G</b>	1060	2,7	11	0,32

#### 4 CONCLUSIONS

A semi-empirical kinetic equation has been proposed that suitably describes the evolution of the degree of sintering advance that a frit particle packing of an exclusively glassy nature undergoes for the whole sintering process, with the heat treatment to which the material is subjected. The fitness of this equation has been demonstrated both in isothermal experiments and in constant-rate-of-heating experiments.

It has been shown, that the marked influence of temperature on the sintering rate of a frit particle packing of an exclusively glassy nature is solely due to the effect of temperature on the viscosity of the molten glass.

Scanning electron microscopy and mercury porsizing were used to analyze the evolution that the porous texture of a frit particle packing underwent with the degree of sintering advance, determining the mechanism, which irrefutably gave rise to sealed pores in the fired material.

On studying the sintering of a glaze prepared from a zirconium frit, it was shown that the devitrifying crystalline phases, which considerably influence frit particle effective viscosity, markedly affect the glaze sintering process. For these kinds of glaze, the densification process can be divided up into three stages or stretches, to each of which the proposed kinetic equation for particles of an exclusively glassy nature is applicable.

It has been shown that glaze particle-size distribution, as it considerably impacts the microstructure of the unfired particle packing, markedly affects not just the rate at which the glaze densifies but also final glaze porosity.

**5 REFERENCES**

- [1] FRENKEL, J. Viscous flow of crystalline bodies under the action of surface tension. *J. Phys.*, 9, 385, 1945.
- [2] KUCZYNSKI, G.C. Study of the sintering of glass. *J. Appl. Phys.*, 20, 1160, 1949.
- [3] MACKENZIE, J.K.; SHUTTLEWORTH, R. A Phenomenological theory of sintering. *Proc. Phys. Soc.*, (London), 62B, 833-52, 1949.
- [4] ZAGAR, L. Sintering of glass powders. *Sci. Sinter.*, 7(1), 37-43, 1975.
- [5] ZAGAR, L. Theoretical aspects of sintering glass powders. En RISTIC, M. (ed.) *Sintering new developments*. Amsterdam: Elsevier, 1979, 57-64.
- [6] KUCZYNSKI, G.C.; ZAPLATYNSKY, J. Sintering of glass. *J. Am. Ceram. Soc.*, 39(10), 349-50, 1956.
- [7] SCHERER, G.W. Sintering of low-density glasses: II. Experimental study. *J. Am. Ceram. Soc.*, 60(5-6), 239-43, 1977.
- [8] SCHERER, G.W. Sintering of low-density glasses: I. Theory. *J. Am. Ceram. Soc.*, 60(5-6), 236-39, 1977.
- [9] GIESS, E.A.; FLETCHER, J.P.; HERRON, L.W. Isothermal sintering of cordierite-type glass powders. *J. Am. Ceram. Soc.*, 67(8), 549-52, 1984.
- [10] BORDIA, R.K.; RAJ, R. Analysis of sintering of a composite with a glass or ceramic matrix. *J. Am. Ceram. Soc.*, 69(3), C55-C57, 1986.
- [11] PETRU, Z. Sinterung von polydispersen Glaspulvern. *Silic. Ind.*, 36(10), 247-253, 1971.
- [12] SACKS, M.D.; VORA, S.D. Preparation of SiO<sub>2</sub> glass from model powder compacts: III, Enhanced densification by sol infiltration. *J. Am. Ceram. Soc.*, 71(4), 245-49, 1988.
- [13] AMOROS, J.L.; ESCARDINO, A.; ORTS, M.J.; MORENO, A. Zirconium glazes used in fast single fired wall tile manufacture: Part 1. Crystallisation mechanism. *Br. Ceram. Trans.*, 93(6), 224-228, 1994.